Structural information in the local electric field of dissolved *B*-DNA

David Hochberg, Thomas W. Kephart, and Glenn Edwards
Department of Physics and Astronomy, Vanderbilt University, Nashville, Tennessee 37235
(Received 10 September 1993)

We have developed a theoretical model of the electric potential and field for *B*-DNA in solution to investigate the persistence of structural information in the local field. A Green-function technique is used to account for the phosphate groups, the dominant charges of the polyelectrolyte DNA, as discrete surface charges exhibiting helical geometry. In addition to the DNA macromolecule, a region of condensed ions and bulk solvent are treated as dielectric media with cylindrical symmetry. We have derived analytical expressions that manifest the symmetry of the system. The leading term is equivalent to that of a continuous line charge and thus only reflects cylindrical symmetry. Information reflecting the helical structure is contained in the terms of higher order. The effective decay length for helical information in the local electric field is approximately 5 Å beyond the surface of DNA. These results have significance for investigations of nucleic-acid–protein interactions and for experimental efforts to image DNA with scanning force microscopies.

PACS number(s): 87.15.−v, 36.20.−r, 41.20.Cv

I. INTRODUCTION

The nature of the DNA-solvent interface has been the subject of ongoing theoretical [1–9] and experimental [10–13] efforts impacting a number of fields including biological physics, polymer physics, and fluid dynamics. DNA is a polyelectrolyte exhibiting helical symmetry with a high density of surface charge due to pairs of phosphate groups with a periodicity of 3.4 Å along the helical axis [14]. The interest in the electrostatic properties of DNA has evolved over the past several decades, ranging from investigations of the physical mechanisms governing gel electrophoresis [4], to the role of the electric potential and electric field in DNA-protein [2] and DNA-DNA [7,10] interactions, to attempts to image DNA with scanning force microscopies [15].

A variety of idealizations have been used in developing theoretical models for the thermodynamic and electrostatic properties of polyelectrolytes due to the inherent complexities of these systems. One class of idealization treats the solvent with versions of either the Debye-Hückel or Poisson-Boltzmann equations, but treats DNA as a continuous charge distribution with cylindrical symmetry [1,4]. Another class of models includes more structural detail of DNA, placing less emphasis on the solvent [2]. A third class of models includes structural details about both DNA and the solvent [8]; however, the length of the DNA macromolecule and the amount of surrounding solvent that can be considered are limited by computational power. In general, each class of theoretical models exhibits definite but limited reliability.

More recently, measurements of DNA systems with controlled amounts of solvent between DNA surfaces have begun to elucidate additional mechanisms governing the interface. Parsegian and co-workers [10] have highlighted the role of water, measuring a repulsive "hydration force" in the near-contact region; Gruen, Marcelja, and Pailthrope [7] have attributed this effect to a surface-induced polarization of the aqueous solvent. In addition to water-based interaction mechanisms, the role of the solvent ions has been highlighted by Manning condensation theory [5] and Edwards, Ying, and Tribble recently measured a dielectric relaxation in DNA gels that is attributed to a counter-ion-based mechanism [13]. These recent results draw attention to the local electric field.

Here we report on our calculations of model DNA with discrete charges in helical geometry. We have undertaken this investigation to address the issue of what structural information exists in the local electric field due to DNA. More specifically, how quickly does the electric field approach that of a featureless, charged cylinder (far field), or within what distance is the helical geometry evident (local or near field)? In the following we present analytical expressions that describe the detailed geometry of the local field and we present plots that quantify the loss of the helical "signature" as a function of distance from the DNA surface. In addition, we also summarize a preliminary consideration regarding the contribution to the local field due to the charge distribution of the bases.

II. CALCULATION OF THE ELECTRIC FIELD

An exact calculation of the electric potential and field for DNA in solution is currently an intractable problem. An idealized model is necessary in order to make progress in understanding the physical mechanisms governing the interface, as well as the properties of DNA in solvent. The dominant charged species of DNA occurs at the phosphate groups, which reside on the backbones of the helical strands, i.e., essentially at the solvent-DNA interface [2,14]. Electric dipole and higher-order charge distributions occur in other regions of the molecule, such as the base pairs. Surrounding the negatively charged DNA is a region of condensed ions [5]. This region is at a molarity of about 2 independent of the molarity of the

surrounding bulklike solvent, which is typically tens of millimolars.

Figure 1 presents the geometry of our model. Figure 1(a) displays the arrangement of charges in one of the DNA helices. Figure 1(b) is the geometry for a single surface charge and for three concentric dielectric cylinders representing the regions of DNA, the condensed ions, and the surrounding solvent, respectively. The boundary between DNA and the Manning cloud [the ϵ_1-ϵ_2 boundary in Fig. 1(b)] contains the surface charge, corresponding to the phosphate groups, exhibiting helical symmetry, as shown in Fig. 1(a).

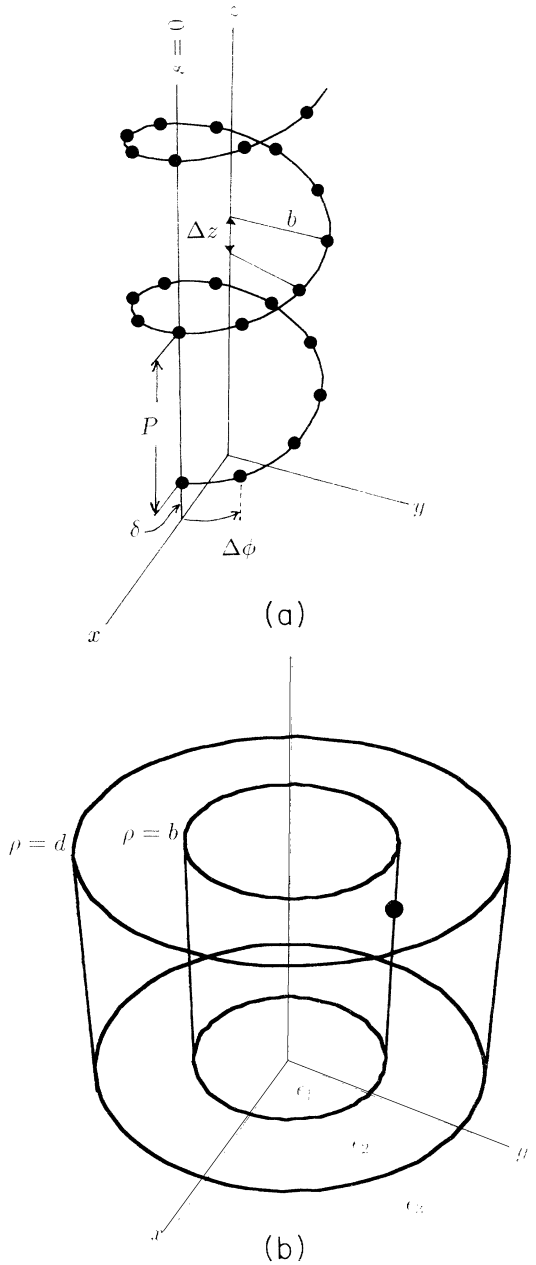

FIG. 1. (a) Geometry of the surface charge distribution. The line marked as $s=0$ identifies one of the ten discrete line charges (see the text). (b) Geometry for a single surface charge embedded in three concentric dielectric media. The dielectric constants ϵ_1, ϵ_2, and ϵ_3 refer to the DNA, Manning cloud, and bulk solvent, respectively.

There are a number of techniques that are traditionally used to solve boundary-value problems in electrostatics [16]. Some of the more familiar come under the heading of solution by conformal mapping, solution by inversion, solution by method of images, separation of variables, and the more general solution by the Green-function method. The practical application of one or more of these techniques depends crucially on the degree of symmetry in the given problem as well as on the effective dimensionality. Neither conformal mapping nor inversion apply to the present case since the former is suited only for two-dimensional systems and the latter for spherical boundaries, while the geometry unique to the helix possesses neither of these attributes. Likewise, the method of images is only useful if one can find a *finite* number of judiciously placed image charges which, together with the real charge (or charges), satisfy the requissite boundary conditions. Again, the helical charge distribution in a cylindrical dielectric medium does not admit a finite number of image charges. Thus, of the techniques mentioned here, the full power of the Green-function approach is required for solving the problem at hand.

It is worthwhile to comment further on the manner in which the helical geometry is included in this model of concentric dielectric cylinders. Although the double-helix configuration of point charges does *not* possess cylindrical symmetry, the helix charges are located on a single cylindrical surface and thus cylindrical coordinates provide the most natural system in which to separate Laplace's operator. As described in complete detail in the Appendixes, the potential for the double helix is obtained by summing the Green function over the helical charge distribution. Note, however, that the sum is broken out as ten sums of discrete line charges at the boundary. Thus this calculation is not a traditional lattice calculation of DNA [17,18], but instead ten displaced line charges in cylindrical symmetry where the configuration of these line charges is equivalent to that of the double helix. This approach proved to be both conceptually simple and calculationally convenient, as will be seen below. The validity of this approach corresponds to the degree that the phosphate groups determine the electric potential and field in the solvent surrounding DNA [2].

The solvent has been modeled as two dielectric regions. While the phosphate groups are essentially bound surface charges, counterions and other solvent ions are free charges. The cylindrical shell of condensed ions accounts for the "charging" near the DNA surface and this relatively high molar region is treated as dielectrically distinct from the bulk solvent. This treatment is supported by previous investigations [5,13].

The model parameters are as follows: The DNA radius $b=10$ Å, the radius of the Manning cloud $d=20$ Å, the helix pitch $P=31.45$ Å, and the vertical rise per charge $\Delta z=3.145$ Å. $N_0=P/\Delta z$ is the number of steps taken along the helix required to complete one period of the helix. The dielectric constants in the three regions are $\epsilon_1=2.0$, $\epsilon_2=50$ (corresponding to $2M$ NaCL), and $\epsilon_3=78$ (corresponding to 10 mM NaCl), respectively.

The phosphate groups are offset a distance $\delta=1.57$ Å from the planes of the base pairs as indicated by a survey of *B*-DNA structures. The mathematical details of the calculation of the potential are presented in the appendixes. Appendix A outlines the calculation of the potential of an infinite discrete helical charge distribution. Appendix B summarizes the calculation of the potential of a point charge in three cylindrically symmetric dielectric media based on the Green-function technique and Fourier expansions.

The exact electric field for the idealized model of DNA is

$$\mathbf{E}=-\left[\hat{\boldsymbol{\rho}}\frac{\partial}{\partial\rho}+\hat{\boldsymbol{\phi}}\frac{1}{\rho}\frac{\partial}{\partial\phi}+\hat{\mathbf{z}}\frac{\partial}{\partial z}\right]\Phi_{\text{double helix}}\ , \tag{2.1}$$

where $\Phi_{\text{double helix}}$ is given in (A26)–(A33). The individual field components in the region $b\le\rho\le d$ are as follows:

$$E_\rho(\rho,\phi,z)=\frac{4q/\epsilon_2}{\Delta z}\frac{1}{\rho}+\frac{8q}{b\Delta z}\sum_{l=1}^{\infty}\cos\left[\frac{2\pi l}{\Delta z}z\right]\cos\left[\frac{2\pi l}{\Delta z}\delta\right]\mathcal{B}_{0,2\pi l/\Delta z}\left[-r_{(0,2\pi l/\Delta z)}I_1\left[\frac{2\pi l}{\Delta z}\rho\right]+K_1\left[\frac{2\pi l}{\Delta z}\rho\right]\right]$$

$$+\frac{8q}{\Delta z}\frac{1}{\rho}\sum_{l=1}^{\infty}\cos(lN_0\phi)\left[\frac{\dfrac{-(\epsilon_2-\epsilon_3)}{\epsilon_3(\epsilon_2+\epsilon_3)}\left[\dfrac{b}{d}\right]^{lN_0}\left[\dfrac{\rho}{d}\right]^{lN_0}+\left[\dfrac{b}{\rho}\right]^{lN_0}}{\dfrac{(\epsilon_1-\epsilon_2)(\epsilon_2-\epsilon_3)}{\epsilon_3(\epsilon_2+\epsilon_3)}\left[\dfrac{b}{d}\right]^{2lN_0}+(\epsilon_1+\epsilon_2)}\right]$$

$$-\frac{8q}{b\Delta z}\sum_{l=1}^{\infty}\left\{\sum_{m=2,\text{even}}^{lN_0-1}\cos\left[\frac{2\pi z}{P}(lN_0-m)+m\phi\right]\cos\left[\frac{2\pi}{P}(lN_0-m)\delta\right]\right.$$

$$\left.-\sum_{m=1,\text{odd}}^{lN_0-1}\sin\left[\frac{2\pi z}{P}(lN_0-m)+m\phi\right]\sin\left[\frac{2\pi}{P}(lN_0-m)\delta\right]\right\}$$

$$\times\mathcal{B}_{m,(2\pi/P)(lN_0-m)}\left[r_{[m,(2\pi/P)(lN_0-m)]}I'_m\left[\frac{2\pi}{P}(lN_0-m)\rho\right]+K'_m\left[\frac{2\pi}{P}(lN_0-m)\rho\right]\right]$$

$$-\frac{8q}{b\Delta z}\sum_{l=-\infty}^{\infty}\left\{\sum_{m=\max[2,2-lN_0],\text{even}}^{\infty}\cos\left[\frac{2\pi z}{P}(lN_0+m)-m\phi\right]\cos\left[\frac{2\pi}{P}(lN_0+m)\delta\right]\right.$$

$$\left.-\sum_{m=\max[1,1-lN_0],\text{odd}}^{\infty}\sin\left[\frac{2\pi z}{P}(lN_0+m)-m\phi\right]\sin\left[\frac{2\pi}{P}(lN_0+m)\delta\right]\right\}$$

$$\times\mathcal{B}_{m,(2\pi/P)(lN_0+m)}\left[r_{[m,(2\pi/P)(lN_0+m)]}I'_m\left[\frac{2\pi}{P}(lN_0+m)\rho\right]+K'_m\left[\frac{2\pi}{P}(lN_0+m)\rho\right]\right],$$

(2.2)

$$E_\phi(\rho,\phi,z)=\frac{8q}{\Delta z}\frac{1}{\rho}\sum_{l=1}^{\infty}\sin(lN_0\phi)\left[\frac{\frac{(\epsilon_2-\epsilon_3)}{\epsilon_3(\epsilon_2+\epsilon_3)}\left[\frac{b}{d}\right]^{lN_0}\left[\frac{\rho}{d}\right]^{lN_0}+\left[\frac{b}{\rho}\right]^{lN_0}}{\frac{(\epsilon_1-\epsilon_2)(\epsilon_2-\epsilon_3)}{\epsilon_3(\epsilon_2+\epsilon_3)}\left[\frac{b}{d}\right]^{2lN_0}+(\epsilon_1+\epsilon_2)}\right]$$

$$+\frac{4qN_0}{b\pi}\frac{1}{\rho}\sum_{l=1}^{\infty}\left\{\sum_{m=2,\text{even}}^{lN_0-1}\sin\left[\frac{2\pi z}{P}(lN_0-m)+m\phi\right]\cos\left[\frac{2\pi}{P}(lN_0-m)\delta\right]\frac{m}{(lN_0-m)}\right.$$

$$\left.+\sum_{m=1,\text{odd}}^{lN_0-1}\cos\left[\frac{2\pi z}{P}(lN_0-m)+m\phi\right]\sin\left[\frac{2\pi}{P}(lN_0-m)\delta\right]\frac{m}{(lN_0-m)}\right\}$$

$$\times\mathcal{B}_{m,(2\pi/P)(lN_0-m)}\left[r_{[m,(2\pi/P)(lN_0-m)]}I_m\left[\frac{2\pi}{P}(lN_0-m)\rho\right]+K_m\left[\frac{2\pi}{P}(lN_0-m)\rho\right]\right]$$

$$+\frac{4qN_0}{b\pi}\frac{1}{\rho}\sum_{l=-\infty}^{\infty}\left\{\sum_{m=\max[2,2-lN_0],\text{even}}^{\infty}\sin\left[\frac{2\pi z}{P}(lN_0+m)-m\phi\right]\cos\left[\frac{2\pi}{P}(lN_0+m)\right]\frac{-m}{(lN_0+m)}\right.$$

$$\left.+\sum_{m=\max[1,1-lN_0],\text{odd}}^{\infty}\cos\left[\frac{2\pi z}{P}(lN_0+m)-m\phi\right]\sin\left[\frac{2\pi}{P}(lN_0+m)\right]\frac{-m}{(lN_0+m)}\right\}$$

$$\times\mathcal{B}_{m,(2\pi/P)(lN_0+m)}\left[r_{[m,(2\pi/P)(lN_0+m)]}I_m\left[\frac{2\pi}{P}(lN_0+m)\rho\right]+K_m\left[\frac{2\pi}{P}(lN_0+m)\rho\right]\right],\tag{2.3}$$

and

$$E_z(\rho,\phi,z)=\frac{8q}{b\Delta z}\sum_{l=1}^{\infty}\sin\left[\frac{2\pi l}{\Delta z}z\right]\cos\left[\frac{2\pi}{\Delta z}\delta\right]\mathcal{B}_{0,2\pi l/\Delta z}\left[r_{(0,2\pi l/\Delta z)}I_0\left[\frac{2\pi l}{\Delta z}\rho\right]+K_0\left[\frac{2\pi l}{\Delta z}\rho\right]\right]$$

$$+\frac{8q}{b\Delta z}\sum_{l=1}^{\infty}\left\{\sum_{m=2,\text{even}}^{lN_0-1}\sin\left[\frac{2\pi z}{P}(lN_0-m)+m\phi\right]\cos\left[\frac{2\pi}{P}(lN_0-m)\delta\right]\right.$$

$$\left.+\sum_{m=1,\text{odd}}^{lN_0-1}\cos\left[\frac{2\pi z}{P}(lN_0-m)+m\phi\right]\sin\left[\frac{2\pi}{P}(lN_0-m)\delta\right]\right\}$$

$$\times\mathcal{B}_{m,(2\pi/P)(lN_0-m)}\left[r_{[m,(2\pi/P)(lN_0-m)]}I_m\left[\frac{2\pi}{P}(lN_0-m)\rho\right]+K_m\left[\frac{2\pi}{P}(lN_0-m)\rho\right]\right]$$

$$+\frac{8q}{b\Delta z}\sum_{l=-\infty}^{\infty}\left\{\sum_{m=\max[2,2-lN_0],\text{even}}^{\infty}\sin\left[\frac{2\pi z}{P}(lN_0+m)-m\phi\right]\cos\left[\frac{2\pi}{P}(lN_0+m)\delta\right]\right.$$

$$\left.+\sum_{m=\max[1,1-lN_0],\text{odd}}^{\infty}\cos\left[\frac{2\pi z}{P}(lN_0+m)-m\phi\right]\sin\left[\frac{2\pi}{P}(lN_0+m)\delta\right]\right\}$$

$$\times\mathcal{B}_{m,(2\pi/P)(lN_0+m)}\left[r_{[m,(2\pi/P)(lN_0+m)]}I_m\left[\frac{2\pi}{P}(lN_0+m)\rho\right]+K_m\left[\frac{2\pi}{P}(lN_0+m)\rho\right]\right],\tag{2.4}$$

while for the region $d \le \rho < \infty$, corresponding to the bulk solvent, we have

$$E_\rho(\rho,\phi,z)=\frac{4q/\epsilon_3}{\Delta z}\frac{1}{\rho}+\frac{8q}{b\Delta z}\sum_{l=1}^{\infty}\cos\left[\frac{2\pi l}{\Delta z}z\right]\cos\left[\frac{2\pi l}{\Delta z}\delta\right]\mathcal{H}_{0,2\pi l/\Delta z}K_1\left[\frac{2\pi l}{\Delta z}\rho\right]$$

$$+\frac{8q}{\Delta z}\frac{1}{\rho}\sum_{l=1}^{\infty}\cos(lN_0\phi)\left[\frac{\frac{(\epsilon_2-\epsilon_3)}{\epsilon_3(\epsilon_2+\epsilon_3)}+1}{\frac{(\epsilon_1-\epsilon_2)(\epsilon_2-\epsilon_3)}{\epsilon_3(\epsilon_2+\epsilon_3)}\left[\frac{b}{d}\right]^{2lN_0}+(\epsilon_1+\epsilon_2)}\right]\left[\frac{b}{\rho}\right]^{lN_0}$$

$$-\frac{8q}{b\Delta z}\sum_{l=1}^{\infty}\left\{\sum_{m=2,\text{even}}^{lN_0-1}\cos\left[\frac{2\pi z}{P}(lN_0-m)+m\phi\right]\cos\left[\frac{2\pi}{P}(lN_0-m)\delta\right]\right.$$

$$\left.-\sum_{m=1,\text{odd}}^{lN_0-1}\sin\left[\frac{2\pi z}{P}(lN_0-m)+m\phi\right]\sin\left[\frac{2\pi}{P}(lN_0-m)\delta\right]\right\}$$

$$\times\mathcal{H}_{m,(2\pi/P)(lN_0-m)}K'_m\left[\frac{2\pi}{P}(lN_0-m)\rho\right]$$

$$-\frac{8q}{b\Delta z}\sum_{l=-\infty}^{\infty}\left\{\sum_{m=\max[2,2-lN_0],\text{even}}^{\infty}\cos\left[\frac{2\pi z}{P}(lN_0+m)-m\phi\right]\cos\left[\frac{2\pi}{P}(lN_0+m)\delta\right]\right.$$

$$\left.-\sum_{m=\max[1,1-lN_0],\text{odd}}^{\infty}\sin\left[\frac{2\pi z}{P}(lN_0+m)-m\phi\right]\sin\left[\frac{2\pi}{P}(lN_0+m)\delta\right]\right\}$$

$$\times\mathcal{H}_{m,(2\pi/P)(lN_0+m)}K'_m\left[\frac{2\pi}{P}(lN_0+m)\rho\right], \tag{2.5}$$

$$E_\phi(\rho,\phi,z)=\frac{8q}{\Delta z}\frac{1}{\rho}\sum_{l=1}^{\infty}\sin(lN_0\phi)\left[\frac{\frac{(\epsilon_2-\epsilon_3)}{\epsilon_3(\epsilon_2+\epsilon_3)}+1}{\frac{(\epsilon_1-\epsilon_2)(\epsilon_2-\epsilon_3)}{\epsilon_3(\epsilon_2+\epsilon_3)}\left[\frac{b}{d}\right]^{2lN_0}+(\epsilon_1+\epsilon_2)}\right]\left[\frac{b}{\rho}\right]^{lN_0}$$

$$+\frac{4qN_0}{b\pi}\frac{1}{\rho}\sum_{l=1}^{\infty}\left\{\sum_{m=2,\text{even}}^{lN_0-1}\sin\left[\frac{2\pi z}{P}(lN_0-m)+m\phi\right]\cos\left[\frac{2\pi}{P}(lN_0-m)\delta\right]\frac{m}{(lN_0-m)}\right.$$

$$\left.+\sum_{m=1,\text{odd}}^{lN_0-1}\cos\left[\frac{2\pi z}{P}(lN_0-m)+m\phi\right]\sin\left[\frac{2\pi}{P}(lN_0-m)\delta\right]\frac{m}{(lN_0-m)}\right\}$$

$$\times\mathcal{H}_{m,(2\pi/P)(lN_0-m)}K_m\left[\frac{2\pi}{P}(lN_0-m)\rho\right]$$

$$+\frac{4qN_0}{b\pi}\frac{1}{\rho}\sum_{l=-\infty}^{\infty}\left\{\sum_{m=\max[2,2-lN_0],\text{even}}^{\infty}\sin\left[\frac{2\pi z}{P}(lN_0+m)-m\phi\right]\cos\left[\frac{2\pi}{P}(lN_0+m)\delta\right]\frac{-m}{(lN_0+m)}\right.$$

$$\left.+\sum_{m=\max[1,1-lN_0],\text{odd}}^{\infty}\cos\left[\frac{2\pi z}{P}(lN_0+m)-m\phi\right]\sin\left[\frac{2\pi}{P}(lN_0+m)\delta\right]\frac{-m}{(lN_0+m)}\right\}$$

$$\times\mathcal{H}_{m,(2\pi/P)(lN_0+m)}K_m\left[\frac{2\pi}{P}(lN_0+m)\rho\right], \tag{2.6}$$

and

$$E_z(\rho,\phi,z)=\frac{8q}{b\Delta z}\sum_{l=1}^{\infty}\sin\left[\frac{2\pi l}{\Delta z}z\right]\cos\left[\frac{2\pi}{\Delta z}\delta\right]\mathcal{K}_{0,2\pi l/\Delta z}K_0\left[\frac{2\pi l}{\Delta z}\rho\right]$$

$$+\frac{8q}{b\Delta z}\sum_{l=1}^{\infty}\left\{\sum_{m=2,\text{even}}^{lN_0-1}\sin\left[\frac{2\pi z}{P}(lN_0-m)+m\phi\right]\cos\left[\frac{2\pi}{P}(lN_0-m)\delta\right]\right.$$

$$\left.+\sum_{m=1,\text{odd}}^{lN_0-1}\cos\left[\frac{2\pi z}{P}(lN_0-m)+m\phi\right]\sin\left[\frac{2\pi}{P}(lN_0-m)\delta\right]\right\}$$

$$\times\mathcal{K}_{m,(2\pi/P)(lN_0-m)}K_m\left[\frac{2\pi}{P}(lN_0-m)\rho\right]$$

$$+\frac{8q}{b\Delta z}\sum_{l=-\infty}^{\infty}\left\{\sum_{m=\max[2,2-lN_0],\text{even}}^{\infty}\sin\left[\frac{2\pi z}{P}(lN_0+m)-m\phi\right]\cos\left[\frac{2\pi}{P}(lN_0+m)\delta\right]\right.$$

$$\left.+\sum_{m=\max[1,1-lN_0],\text{odd}}^{\infty}\cos\left[\frac{2\pi z}{P}(lN_0+m)-m\phi\right]\sin\left[\frac{2\pi}{P}(lN_0+m)\delta\right]\right\}$$

$$\times\mathcal{K}_{m,(2\pi/P)(lN_0+m)}K_m\left[\frac{2\pi}{P}(lN_0+m)\rho\right]. \tag{2.7}$$

Here, I_m and K_m are modified Bessel functions and the functions $r_{(m,k)}$, $\mathcal{B}$, and $\mathcal{K}$ are given in (B14), (B21), and (B22).

A few remarks pertaining to these expressions are in order. First, note that the leading-order term in E_ρ is the familiar $1/\rho$ term which is what we expect for a line charge. The rest of the terms in E_ρ may therefore be regarded as "corrections" to the line-charge contribution arising from the helical geometry of the charge distribution. Likewise, both E_ϕ and E_z vanish identically for a pure line charge; hence, *all* terms appearing in (2.3), (2.4), (2.6), and (2.7) are due to the helical geometry of the charge distribution.

The full expressions are somewhat cumbersome, and we have computed values of the electric field using MATHEMATICA running on a Quadra 700. However, it is instructive to make some estimates of the range of the various correction terms which, after all, are the signature of the helical structure. Each of the ρ-dependent parts of the summands appearing in the infinite series expressions are of similar form [e.g., see (2.10) below] for all field components; we will focus on those corresponding to E_ρ for the intermediate region defined by $b\le\rho\le d$. The extent (in ρ) of the correction terms is dominated by the longest wavelength in the problem, which is in turn, given by the reciprocal of the smallest wave number k. Inspection of the various terms in (2.2) indicates that the value of the repeat length of the charge configuration (and which takes δ into account) in the z-direction is $(k_{\min})^{-1}=P/2\pi$, which follows directly from consideration of the constrained double sums. This corresponds to a length scale of ≈ 5 Å. We therefore expect the decay length of the dominant corrections of all the field components to be of the order of about 5 Å from the DNA surface. An estimate of the leading ρ-dependent correction term in the sum confirms this behavior. Indeed, using the asymptotic expansions [19] (note the leading-order terms are independent of the order m of the Bessel functions),

$$I_m(w)\sim\frac{e^w}{\sqrt{2\pi w}}[1+O(w^{-1})], \tag{2.8}$$

$$K_m(w)\sim\left[\frac{\pi}{2w}\right]^{1/2}e^{-w}[1+O(w^{-1})] \tag{2.9}$$

[the corresponding form for $K'_m(w)$ is obtained from (2.9) simply by multiplying that by -1], we can show that $k_{\min}$ sets the scale for the corrections. Consider a typical term of the form

$$r_{(m,k)}I'_m(k\rho)+K'_m(k\rho). \tag{2.10}$$

From the definition of r in (B14) and using the above expansions, we have

$$r_{(m,k)}I'_m(k\rho)\sim\pi\left[\frac{\epsilon_3-\epsilon_2}{\epsilon_3+\epsilon_2}\right]e^{-2kd}\frac{e^{k\rho}}{\sqrt{2\pi k\rho}}[1+O(kd)^{-1}]. \tag{2.11}$$

This is maximized for $\rho=d$ since I_m is an increasing function of its argument. The point is that (2.11) becomes proportional to a decaying exponential e^{-kd}, with decay length $k^{-1}\sim 5$ Å. Similarly, from (2.9), we see that $K'_m(k_{\min}\rho)$ decays like $e^{-k\rho}/\sqrt{k\rho}$ and, hence, so does (2.10).

Now let us discuss the symmetry properties of the sur-

face charge distribution. The electric potential and field derived here are invariant under a set of five discrete transformations. They are as follows: translations in the z direction by multiples of P:

$$\text{(i)}\quad z \rightarrow z+P\ , \tag{2.12}$$

rotations and shifts:

$$\text{(ii)}\quad \phi \rightarrow \phi+\pi\ ,\quad z+\delta \rightarrow z-\delta\ ; \tag{2.13}$$

the so-called helical transformation:

$$\text{(iii)}\quad z \rightarrow z+\Delta z \quad \text{and} \quad \phi \rightarrow \phi+\Delta\phi\ ; \tag{2.14}$$

where $\Delta\phi = 2\pi/N_0$ and $\Delta z = P/N_0$; and finally, the "baton-twirl" symmetry. Every $z=$const slice containing a base pair, e.g., $z=0$, or lying midway between base pairs, e.g., $z=\Delta z/2$, exhibits twofold symmetry. This is easiest to see in the $z=0$ plane where the field is invariant under the transformation corresponding to a rotation about the C_2 symmetry axis:

$$\text{(iv)}\quad \phi \rightarrow \pi-\phi \quad \text{and} \quad z \rightarrow -z\ . \tag{2.15}$$

For the $z=\Delta z/2$ plane, the rotation is about the dyad axis:

$$\text{(v)}\quad \phi \rightarrow (\pi+\pi/10)-\phi \quad \text{and} \quad z \rightarrow -z\ . \tag{2.16}$$

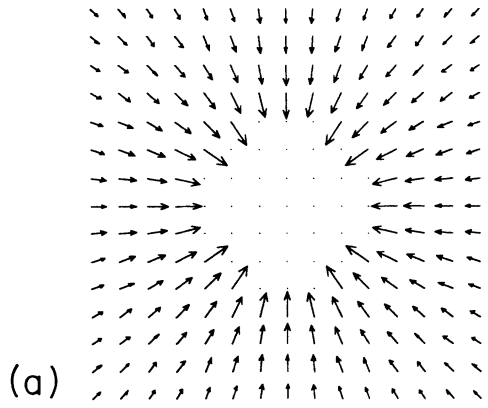

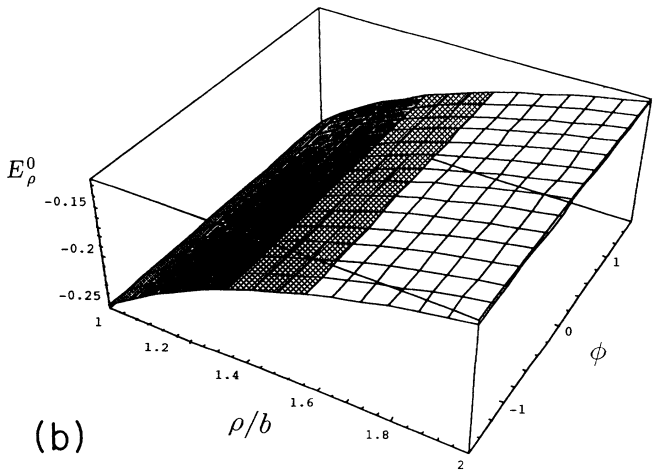

FIG. 2. Plot of the electric field of the leading term in $\mathbf{E}_\rho, \mathbf{E}^0_\rho$: (a) is a vector plot and (b) is a surface plot of the $z=0$ plane. Note that in (b) the ρ axis is normalized by b.

III. RESULTS

The leading term for E_ρ is given in (2.2) and (2.5) and is equivalent to that of a line charge, as shown in Fig. 2. Figures 3 and 4 present the subsequent terms for E_ρ and the components E_ϕ as given in (2.3) and (2.6) and E_z as given in (2.4) and (2.7): These correction terms are presented relative to the magnitude of the line-charge term to emphasize the magnitude of the helical signature. Figure 3 refers to the field in the base plane at $z=0$ plotted from $\phi=-\pi/2$ to $\pi/2$. Figure 4 refers to a plane at $z=\Delta z/2$, plotted from $\phi=-9\pi/20$ to $11\pi/20$, planes midway between the base pairs. Note that the surface and contour plots depict slices of cylindrical shells in Cartesian coordinates where $\rho/b=1$ corresponds to the DNA surface.

Note the influence of neighboring phosphate groups, which are spaced by 36°, in the fields plotted in Figs. 3 and 4. Furthermore, inspection of Figs. 2 through 4 reveals more structure closer to the DNA surface; this is, of course, due to the shorter decay lengths for the higher-order terms as given in (2.2)–(2.8).

IV. DISCUSSION

Care must be taken in interpreting these results due to the idealizations of this theoretical model. For example, the geometry is that of an infinitely long and mathematically straight cylinder with a helical charge distribution at the interface. While DNA has a significant persistence length, some of the symmetrical features must still be viewed as approximate. In addition, the solvent has been treated as concentric dielectric cylinders. The DNA-solvent interface is governed by a number of mechanisms which in this model have more or less been folded into dielectric theory, subject to the limitations of linear-response theory. Deviations from dielectric theory may alter our quantitative results; however, our qualitative conclusions should remain valid. Another concern is the treatment of the macromolecule as a cylinder, i.e., the major and minor grooves have been ignored. This is a region where the charge distributions of the bases become important and will be discussed below. The reliable region for this model begins a few angstroms beyond the DNA surface.

The results shown in Figs. 1 through 4 can be considered in terms of length scales. At distances far from the DNA surface, the electric potential and field are that of a line charge embedded in dielectric media, as is to be expected. Within 10 Å of the surface, however, there is significant structural information in the electric field due

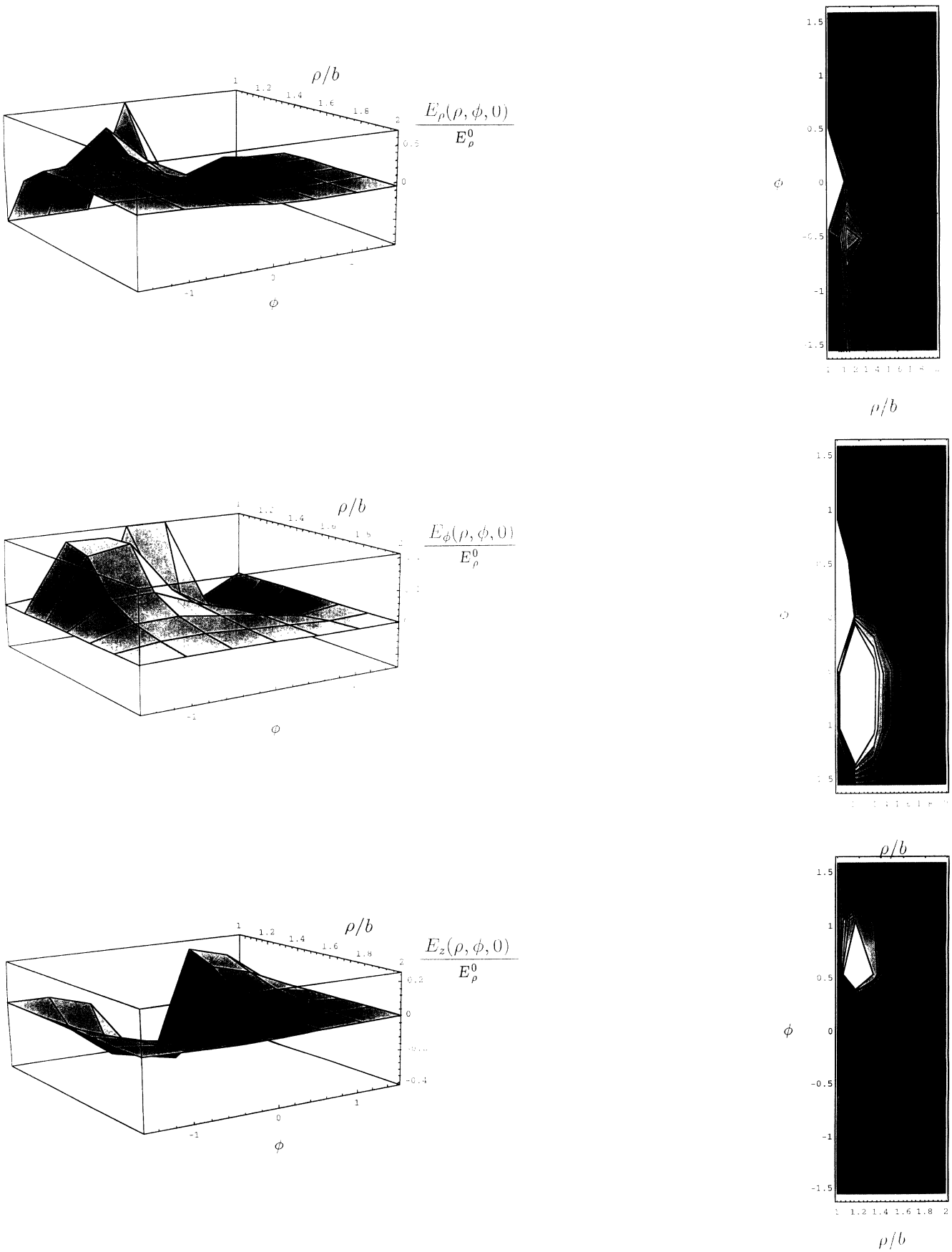

FIG. 3. Surface and contour plots of the components of the correction terms of the electric field in the $z=0$ plane. Note that the intensities of the components are relative to the intensity of the line-charge or zero-mode term E^0_ρ as shown in Fig. 2.

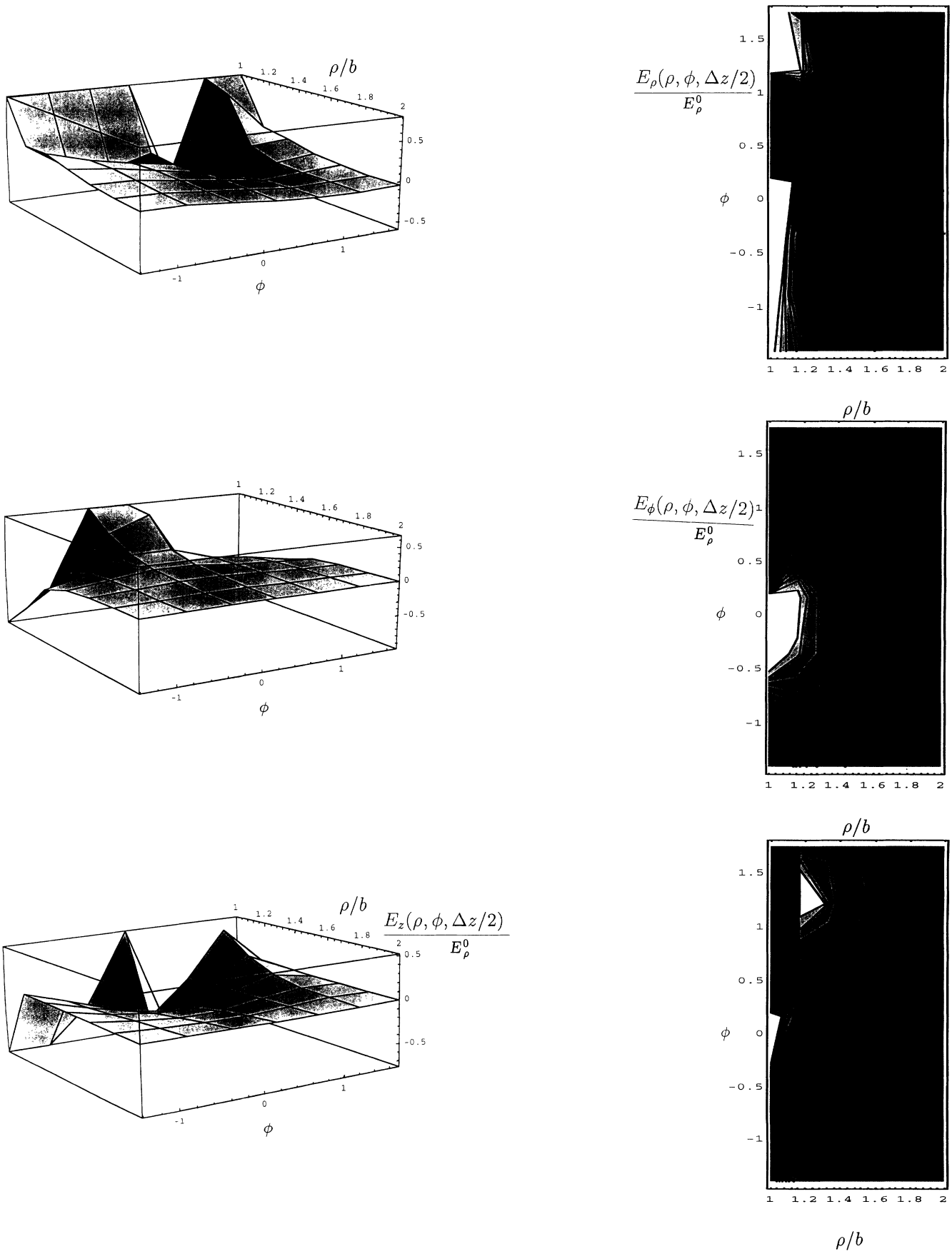

FIG. 4. Surface and contour plots of the components of the correction terms of the electric field in the $z = \Delta z/2$ plane.

to the detailed geometry of the helix. Except at the location of the surface charges where there is a singularity, the magnitude of these correction terms approaches two-thirds that of the line-charge contribution. Furthermore, there is increasing structure with approach to the DNA surface: The effective decay length of this structure is about 5 Å which is significant for the interaction of DNA with other (macro)molecules. Of course, one expects both the potential and electric-field components to diverge at the sites of the point charges. This divergence is prevented in our calculations by taking a finite number (≈ 100) of terms in our Fourier-Bessel expansions. This turned out to give adequate estimates, typically valid within a few percent, for the entire near-field region excluding the charge sites.

It is intriguing to consider the detailed geometry of the local electric field as calculated here with regards to the dynamics of the DNA-solvent interface and DNA-DNA and DNA-protein interactions. In addition, there has been an ongoing experimental effort to probe the local electric field with scanning probe microscopies; our theoretical results indicate experimental length scales for first accessing cylindrical and then helical information with approach to the DNA surface. Note that the sugars and the bases will, in general, also make an electrostatic contribution. The charge distributions for these subunits have been calculated [2,20] and the dipole moments of the bases are quite distinctive. It should be recognized, however, that the progress we have made in carrying out these calculations is due to symmetry; expanding this model to include the dipole and higher-order moments for a nontrivial sequence of bases is possible. Currently we are extending this calculation to investigate the possibility of a distinctive signature in the local electric field attributable to the charge distribution of a given base.

To conclude, we have derived analytical expressions for the electric potential and field to investigate the effect of the helical geometry on the local field near *B*-DNA. Helical information is a significant component of the local field and is characterized by an effective decay length of 5 Å beyond the DNA surface.

ACKNOWLEDGMENTS

This work was supported in part by the Office of Naval Research through Contract No. ONR-N00014-91-0109.

APPENDIX A: POTENTIAL OF AN INFINITE DISCRETE HELICAL CHARGE DISTRIBUTION

The potential in cylindrical coordinates (ρ,ϕ,z) from an extended charge source whose charges are distributed along the interface boundary located at $\rho=b$ [Figs. 1(a) and 1(b)] can be obtained in a mostly straightforward manner by summing the single-charge potentials. The calculation of the single-charge potential is summarized in Appendix B. The linearity of Maxwell's equations allows this "reductionist" approach whereby the potential for a charged double helix immersed in a given medium is built up from the single-charge potentials computed for the same medium (we assume for simplicity that the response of the medium is linear as well, i.e., we ignore back-reaction effects). The potential for a unit charge satisfying prescribed boundary conditions is the Green function. As discussed in Sec. II, the Green-function method is uniquely suited for our application. In building up the complete double-helix potential, our strategy is to regard the single helix of evenly spaced point charges as a two-dimensional regular lattice wrapped around the cylinder $\rho=b$. Then, instead of summing the charges *along* the helix, we first decompose this lattice into a finite collection of one-dimensional vertical line-charge distributions that run parallel to the z axis and sum over all the charges in one such line, and then sum over the finite collection of these one-dimensional chains. This procedure yields the potential for a single infinite helix of point charges. The second helix is accounted for by reflecting through the longitudinal axis, essentially doubling the single-helix expression. We shall use (B23)–(B25) as the starting point for constructing the potential from an infinite, discretely charged (double) helix, which represents an idealization of DNA.

Take the helix axis coincident with the z axis. P is the pitch, Δz is the vertical rise per residue, and $N_0=P/\Delta z$ is the number of steps taken along the helix required to complete one period of the helix. Without loss of generality, fix the location of the "origin" charge at $(b,0,0)$, i.e., translate the coordinate system of Fig. 1(a) by $z\rightarrow z+\delta$. As outlined above, we represent the infinite discrete helix of point charges as a finite collection of infinite vertical discrete line-charge distributions, each of which is located at $\rho=b$. These line-charge distributions are equally spaced in the ϕ direction with constant angular separation $\Delta\phi=2\pi/N_0$, corresponding to the location of the phosphate groups. Such a decomposition facilitates the derivation of the helix potential: The sum over the finite number of vertical chains leads to a simple set of geometric constraints reflecting the helical nature of the charge distribution which are easy to incorporate into our final expressions. We note that the position of the nth charge on the sth vertical chain with fixed angular coordinate ϕ_s is $(b,\phi_s,z_{n,s})$, where

$$z_{n,s}=nP+s\Delta z \ , \tag{A1}$$

$$\phi_s=\left\lfloor\frac{2\pi}{N_0}\right\rfloor s \ , \tag{A2}$$

with $0\le s\le(N_0-1)$ and $-\infty<n<\infty$. For example, with $s=0$,

$$\{(b,0,nP)\,|-\infty<n<\infty\}$$

corresponds to the vertical chain located at $\rho=b$ and $\phi=0$. The separation between its adjacent charges is $z_{n+1,0}-z_{n,0}=P$. The "next" chain ($s=1$) is located at $\rho=b$ and $\phi=2\pi/N_0$. Adjacent charges on this chain are also separated by an amount P, but $z_{n,1}-z_{n,0}=\Delta z$, which represents the vertical rise per charge along the helix. There are N_0 vertical line-charge distributions making up the complete helix ($N_0=10$ for *B*-DNA and $N_0=11$ for *A*-DNA). For $s=N_0$, it follows from (A1) and (A2) that $z_{n,N_0}=(n+1)P$ and $\phi_{N_0}=2\pi$, reflecting the fact that after N_0 "steps" through the angular displacement

$\Delta\phi = 2\pi/N_0$, one arrives at the location of the $(n+1)$th charge at a distance P above the nth charge on the *same* chain.

The single-helix potential is obtained by replacing $z' \to z_{n,s}$ and $\phi' \to \phi_s$ in the single-charge potentials (B23)–(B25) and summing over n and s (for a helix with equal charges q at the residue sights). The sum on n (for fixed s) builds up one infinite vertical line charge, and is effected by means of the Poisson summation formula [21]

$$\sum_{n=-\infty}^{\infty} \cos\{k[z-(nP+s\Delta z)]\} = \frac{2\pi}{P}\cos(k[z-s\Delta z]) \sum_{j=-\infty}^{\infty} \delta\left[k-\frac{2\pi j}{P}\right], \quad \text{(A3)}$$

which allows one to carry out the k integrations immediately, but care must be taken in treating the limits as $k \to 0$ implied by the $j=0$ contribution in (A3). We shall outline the major steps required for computing the potential, focusing our attention on Φ_2, where the subscript 2 indicates the intermediate layer in the model. The development of the helix potential in the other two regions ($0 \le \rho \le b$ and $d \le \rho$) makes use of similar manipulations.

Having summed over n using (A3), the resulting line-charge potential depends on s which serves to label the vertical chain. We make this explicit by writing Φ_2^s. It will be convenient both conceptually and computationally to split off the zero-mode ($m=0$, $k=0$) contribution from the higher-mode terms; thus,

$$\Phi_2^s = \Phi_2^s(m=0,k=0) + \Phi_2^s(m=0,k>0) + \Phi_2^s(m\ge 1,k=0) + \Phi_2^s(m\ge 1,k>0) . \quad \text{(A4)}$$

We note from (B23)–(B25) that the (single-chain) potential Φ^s involves a double-mode (sum over $m \ge 1$, integrate over $k>0$) expansion and the decomposition in (A4) follows from expanding these modes out as indicated using (A3). Physically, each fixed mode probes a specific angular separation and length scale. The m modes reflect the angular separation, while the k modes reflect the scale of structure in the z direction [note that $k \sim (2\pi/P)$].

We turn to the $m=k=0$ mode in (B24) and (A4) and evaluate the small-k limit [the $j=0$ term from (A3)]:

$$\lim_{k\to 0} \frac{1}{2k} \mathcal{B}_{(0,k)}[r_{(0,k)} I_0(k\rho) + K_0(k\rho)]\cos(k[z-s\Delta z]) , \quad \text{(A5)}$$

where the factor of $\frac{1}{2}$ comes from the formal identity

$$\int_0^\infty dk\, f(k)\delta(k) = \tfrac{1}{2} f(0) . \quad \text{(A6)}$$

This requires the limiting forms for the modified Bessel functions of fixed order m and small argument $w \to 0$ [19]:

$$I_m(w) \to \frac{(w/2)^m}{\Gamma(m+1)} , \quad m \ge 0 \quad \text{(A7)}$$

$$K_m(w) \to \tfrac{1}{2}\Gamma(m)(w/2)^{-m} , \quad m \ge 1 \quad \text{(A8)}$$

$$K_0(w) \to -\ln(w) , \quad m=0 . \quad \text{(A9)}$$

Using (A7)–(A9) in (B14), (B21), and (A5), we find that the expression (A5) becomes

$$\frac{b}{2\epsilon_2}\left[-\ln(\rho) - \ln(k) + \left[\frac{\epsilon_3-\epsilon_2}{\epsilon_3}\right]\ln(kd)\right] , \quad \text{(A10)}$$

for small k. As expected, a logarithmic divergence appears as $k \to 0$ and is due to the fact we have considered an infinitely long cylinder. In textbook calculations of the electric field from an infinite line charge, mention of this particular divergence is avoided either by computing the electric field directly (without recourse to a potential) or by truncating the line charge to have a finite length L, computing the field therefrom, and then taking the limit $L \to \infty$. In either case the electric field is always finite and well defined. Indeed, the divergent constant appearing in (A10) can be safely discarded since, as usual, the potential is only defined up to an additive constant—that is to say, only *differences* in the potential are physically relevant [the constant in (A10) is annihilated by the gradient]. We therefore replace the expression (A10) with

$$-\frac{b}{2\epsilon_2}\ln(\rho) . \quad \text{(A11)}$$

Next, we calculate the $k \to 0$ limit implied in the $(m \ge 1,\ k=0)$ contribution in (A4). Using the limiting forms given in (A7)–(A9) with (B14) and (B21), we find, after some tedious but straightforward algebra, that

$$\lim_{k\to 0} \frac{1}{2k} \mathcal{B}_{(m,k)}[r_{(m,k)} I_m(kp) + K_m(kp)]\cos(k[z-s\Delta z]) = \frac{b}{2}\left[\frac{\frac{(\epsilon_2-\epsilon_3)}{\epsilon_3(\epsilon_2+\epsilon_3)}\frac{1}{m}\left[\frac{b}{d}\right]^m\left[\frac{\rho}{d}\right]^m + \frac{1}{m}\left[\frac{b}{\rho}\right]^m}{\frac{(\epsilon_1-\epsilon_2)(\epsilon_2-\epsilon_3)}{\epsilon_3(\epsilon_2+\epsilon_3)}\left[\frac{b}{d}\right]^{2m} + (\epsilon_1+\epsilon_2)}\right] . \quad \text{(A12)}$$

This is to be substituted into the expression for the $(m \ge 1,\ k=0)$ contribution in (A4). For the remaining terms in (A4), one simply replaces $k \to 2\pi j/P$ and sums over all $j \ge 1$. The sum over negative j does not contribute since $k \ge 0$.

The potential for one complete helix follows from summing over the N_0 vertical line charges:

$$\Phi_{\text{helix}} = \sum_{s=0}^{N_0-1} \Phi^s . \quad \text{(A13)}$$

These finite sums can be carried out in closed form by means of the following identities;

$$\sum_{s=0}^{N_0-1} \cos\left[\frac{2\pi j}{P}[z-s\Delta z]\right] = N_0 \cos\left[\frac{2\pi j z}{P}\right]\delta_{j,lN_0} , \quad \text{(A14)}$$

$$\sum_{s=0}^{N_0-1} \cos\left[m\left[\phi - \frac{2\pi s}{N_0}\right]\right] = N_0 \cos(m\phi)\delta_{m,lN_0} , \quad \text{(A15)}$$

and

$$\sum_{s=0}^{N_0-1}\cos\left[\frac{2\pi j}{P}[z-s\Delta z]\right]\cos\left[m\left[\phi-\frac{2\pi s}{N_0}\right]\right]$$
$$=\frac{N_0}{2}\left[\cos\left[\frac{2\pi j}{P}z+m\phi\right]\delta_{(j+m),lN_0}+\cos\left[\frac{2\pi j}{P}z-m\phi\right]\delta_{(j-m),lN_0}\right], \quad \text{(A16)}$$

for integer l, $-\infty<l<\infty$. Because of the Kronecker δ's appearing in (A14)–(A16), the sums over j in (A13) will be replaced by sums over l. Note that the last identity (A16) implies constrained double sums for the ($m\geq 1$, $k>0$) modes. The cosine factors in (A16) couple together the z and ϕ dependences and are both invariant under the coupled set of transformations $z\rightarrow z+P/N_0$ and $\phi\rightarrow\phi+2\pi/N_0$. The pure zero-mode part of (A13) is simply

$$\phi_{2,\text{helix}}(m=0,k=0)=-N_0\frac{2q/\epsilon_2}{P}\ln(\rho)\ . \quad \text{(A17)}$$

Summing the second term in (A4) over s using (A14) gives

$$\Phi_{2,\text{helix}}(m=0,k>0)=\frac{2q}{b\pi}\sum_{l=1}^{\infty}\frac{1}{l}\cos\left[\frac{2\pi l}{\Delta z}z\right]\times\mathcal{B}_{0,2\pi l/\Delta z}\left[r_{(0,2\pi l/\Delta z)}I_0\left[\frac{2\pi l}{\Delta z}\rho\right]+K_0\left[\frac{2\pi l}{\Delta z}\rho\right]\right]\ . \quad \text{(A18)}$$

The third term in (A4) sums to the following expression:

$$\Phi_{2,\text{helix}}(m\geq 1,k=0)=\frac{4q}{P}\sum_{l=1}^{\infty}\cos(lN_0\phi)\left[\frac{\frac{(\epsilon_2-\epsilon_3)}{\epsilon_3(\epsilon_2+\epsilon_3)}\frac{1}{l}\left[\frac{b}{d}\right]^{lN_0}\left[\frac{\rho}{d}\right]^{lN_0}+\frac{1}{l}\left[\frac{b}{\rho}\right]^{lN_0}}{\frac{(\epsilon_1-\epsilon_2)(\epsilon_2-\epsilon_3)}{\epsilon_3(\epsilon_2+\epsilon_3)}\left[\frac{b}{d}\right]^{2lN_0}+(\epsilon_1+\epsilon_2)}\right]\ . \quad \text{(A19)}$$

In implementing the constraints implied by the identity in (A16), we take m to be the independent sum variable and j to be the dependent variable. Then, the constraint $\delta_{(j+m),lN_0}$ together with the fact that $m\geq 1$ and $j\geq 1$ implies $j=(lN_0-m)\geq 1$. But $N_0>0$, so we must have $l\geq 1$, and thus $1\leq m\leq(lN_0-1)$. Likewise, the other constraint $\delta_{(j-m),lN_0}$ together with $m\geq 1$ and $j\geq 1$ implies $m\geq(1-lN_0)\geq 1$. This time, there is no restriction on l, but m is bounded below: $m\geq\max[1,1-lN_0]$, as the reader can verify. Thus, the higher-mode contributions take the following form:

$$\Phi_{2,\text{helix}}(m\geq 1,k>0)=\frac{2qN_0}{b\pi}\sum_{l=1}^{\infty}\sum_{m=1}^{lN_0-1}\cos\left[\frac{2\pi z}{P}(lN_0-m)+m\phi\right]\times\frac{1}{lN_0-m}\mathcal{B}_{m,(2\pi/P)(lN_0-m)}\left[r_{[m,(2\pi/P)(lN_0-m)]}I_m\left[\frac{2\pi}{P}(lN_0-m)\rho\right]+K_m\left[\frac{2\pi}{P}(lN_0-m)\rho\right]\right]$$
$$+\frac{2qN_0}{b\pi}\sum_{l=-\infty}^{\infty}\sum_{m=\max[1,1-lN_0]}^{\infty}\cos\left[\frac{2\pi z}{P}(lN_0+m)-m\phi\right]\times\frac{1}{lN_0+m}\mathcal{B}_{m,(2\pi/P)(lN_0+m)}\left[r_{[m,(2\pi/P)(lN_0+m)]}I_m\left[\frac{2\pi}{P}(lN_0+m)\rho\right]+K_m\left[\frac{2\pi}{P}(lN_0+m)\rho\right]\right]\ . \quad \text{(A20)}$$

The potential for the region $d<\rho$ is given by Φ_3. Carrying out the same steps as for Φ_2, we obtain the single-helix potential $\Phi_{3,\text{helix}}$, where

$$\Phi_{3,\text{helix}}(m=0,k=0)=-N_0\frac{2q/\epsilon_3}{P}\ln(\rho)\ , \quad \text{(A21)}$$

$$\Phi_{3,\text{helix}}(m=0,k>0)=\frac{2q}{b\pi}\sum_{l=1}^{\infty}\frac{1}{l}\cos\left[\frac{2\pi l}{\Delta z}z\right]\mathcal{H}_{0,2\pi l/\Delta z}K_0\left[\frac{2\pi l}{\Delta z}\rho\right]\ , \quad \text{(A22)}$$

$$\Phi_{3,\text{helix}}(m\geq 1,k=0)=\frac{4q}{P}\sum_{l=1}^{\infty}\cos(lN_0\phi)\left[\frac{\frac{(\epsilon_2-\epsilon_3)}{\epsilon_3(\epsilon_2+\epsilon_3)}+1}{\frac{(\epsilon_1-\epsilon_2)(\epsilon_2-\epsilon_3)}{\epsilon_3(\epsilon_2+\epsilon_3)}\left[\frac{b}{d}\right]^{2lN_0}+(\epsilon_1+\epsilon_2)}\right]\frac{1}{l}\left[\frac{b}{\rho}\right]^{lN_0}, \tag{A23}$$

$$\Phi_{3,\text{helix}}(m\geq 1,k>0)=\frac{2qN_0}{b\pi}\sum_{l=1}^{\infty}\sum_{m=1}^{lN_0-1}\cos\left[\frac{2\pi z}{P}(lN_0-m)+m\phi\right]\frac{1}{lN_0-m}\mathcal{K}_{m,(2\pi/P)(lN_0-m)}K_m\left[\frac{2\pi}{P}(lN_0-m)\rho\right]$$
$$+\frac{2qN_0}{b\pi}\sum_{l=-\infty}^{\infty}\sum_{m=\max[1,1-lN_0]}^{\infty}\cos\left[\frac{2\pi z}{P}(lN_0+m)-m\phi\right]$$
$$\times\frac{1}{lN_0+m}\mathcal{K}_{m,(2\pi/P)(lN_0+m)}K_m\left[\frac{2\pi}{P}(lN_0+m)\rho\right]. \tag{A24}$$

The double-helix potential is obtained from the single-helix one according to

$$\Phi_{\text{double helix}}(\rho,\phi,z)=\Phi_{\text{helix}}(\rho,\phi,z+\delta)+\Phi_{\text{helix}}(\rho,\phi+\pi,z-\delta), \tag{A25}$$

where we have returned to the coordinate system of Fig. 1(a). Note that $\Phi_{\text{helix}}(\rho,\phi,z+\delta)$ describes the contribution from the single helix with phosphate groups offset by an amount δ above the plane of the base planes as shown in Fig. 1(a). $\Phi_{\text{helix}}(\rho,\phi+\pi,z-\delta)$ describes the contribution from the complementary helix where the phosphate groups are offset by $-\delta$ [see Eq. (2.13)]. Naturally, the resulting expressions (A26)–(A33) have terms similar to those of the single helical potential derived above, with modifications due to the interference of the two single-helix potentials. They are

$$\Phi_{2,\text{double helix}}(m=0,k=0)=-N_0\frac{4q/\epsilon_2}{P}\ln(\rho), \tag{A26}$$

$$\Phi_{3,\text{double helix}}(m=0,k=0)=-N_0\frac{4q/\epsilon_3}{P}\ln(\rho), \tag{A27}$$

$$\Phi_{2,\text{double helix}}(m=0,k>0)=\frac{4q}{b\pi}\sum_{l=1}^{\infty}\frac{1}{l}\cos\left[\frac{2\pi l}{\Delta z}\delta\right]\cos\left[\frac{2\pi l}{\Delta z}z\right]\mathcal{B}_{0,2\pi l/\Delta z}\left[r_{(0,2\pi l/\Delta z)}I_0\left[\frac{2\pi l}{\Delta z}\rho\right]+K_0\left[\frac{2\pi l}{\Delta z}\rho\right]\right], \tag{A28}$$

$$\Phi_{3,\text{double helix}}(m=0,k>0)=\frac{4q}{b\pi}\sum_{l=1}^{\infty}\frac{1}{l}\cos\left[\frac{2\pi l}{\Delta z}z\right]\cos\left[\frac{2\pi l}{\Delta z}\delta\right]\mathcal{H}_{0,2\pi l/\Delta z}K_0\left[\frac{2\pi l}{\Delta z}\rho\right], \tag{A29}$$

$$\Phi_{2,\text{double helix}}(m\geq 1,k=0)=\frac{8q}{P}\sum_{l=1}^{\infty}\cos(lN_0\phi)\left[\frac{\frac{(\epsilon_2-\epsilon_3)}{\epsilon_3(\epsilon_2+\epsilon_3)}\frac{1}{l}\left[\frac{b}{d}\right]^{lN_0}\left[\frac{\rho}{d}\right]^{lN_0}+\frac{1}{l}\left[\frac{b}{\rho}\right]^{lN_0}}{\frac{(\epsilon_1-\epsilon_2)(\epsilon_2-\epsilon_3)}{\epsilon_3(\epsilon_2+\epsilon_3)}\left[\frac{b}{d}\right]^{2lN_0}+(\epsilon_1+\epsilon_2)}\right], \tag{A30}$$

$$\Phi_{3,\text{double helix}}(m\geq 1,k=0)=\frac{8q}{P}\sum_{l=1}^{\infty}\cos(lN_0\phi)\left[\frac{\frac{(\epsilon_2-\epsilon_3)}{\epsilon_3(\epsilon_2+\epsilon_3)}+1}{\frac{(\epsilon_1-\epsilon_2)(\epsilon_2-\epsilon_3)}{\epsilon_3(\epsilon_2+\epsilon_3)}\left[\frac{b}{d}\right]^{2lN_0}+(\epsilon_1+\epsilon_2)}\right]\frac{1}{l}\left[\frac{b}{\rho}\right]^{lN_0}, \tag{A31}$$

$$\Phi_{2,\text{double helix}}(m \geq 1, k > 0)$$
$$= \frac{4qN_0}{b\pi} \sum_{l=1}^{\infty} \left\{ \sum_{m=2,\text{even}}^{lN_0-1} \cos\left[\frac{2\pi z}{P}(lN_0-m)+m\phi\right] \cos\left[\frac{2\pi}{P}(lN_0-m)\delta\right] \right.$$
$$\left. - \sum_{m=1,\text{odd}}^{lN_0-1} \sin\left[\frac{2\pi z}{P}(lN_0-m)+m\phi\right] \sin\left[\frac{2\pi}{P}(lN_0-m)\delta\right] \right\}$$
$$\times \frac{1}{lN_0+m} \mathcal{B}_{m,(2\pi/P)(lN_0+m)} \left[r_{[m,(2\pi/P)(lN_0-m)]} I_m\left[\frac{2\pi}{P}(lN_0-m)\rho\right] + K_m\left[\frac{2\pi}{P}(lN_0-m)\rho\right] \right]$$
$$+ \frac{4qN_0}{b\pi} \sum_{l=-\infty}^{\infty} \left\{ \sum_{m=\max[2,2-lN_0],\text{even}}^{\infty} \cos\left[\frac{2\pi z}{P}(lN_0+m)-m\phi\right] \cos\left[\frac{2\pi}{P}(lN_0+m)\delta\right] \right.$$
$$\left. - \sum_{m=\max[1,1-lN_0],\text{odd}}^{\infty} \sin\left[\frac{2\pi z}{P}(lN_0+m)-m\phi\right] \sin\left[\frac{2\pi}{P}(lN_0+m)\delta\right] \right\}$$
$$\times \frac{1}{lN_0+m} \mathcal{B}_{m,(2\pi/P)(lN_0+m)} \left[r_{[m,(2\pi/P)(lN_0+m)]} I_m\left[\frac{2\pi}{P}(lN_0+m)\rho\right] + K_m\left[\frac{2\pi}{P}(lN_0+m)\rho\right] \right], \tag{A32}$$

and

$$\Phi_{3,\text{double helix}}(m \geq 1, k > 0)$$
$$= \frac{4qN_0}{b\pi} \sum_{l=1}^{\infty} \left\{ \sum_{m=2,\text{even}}^{lN_0-1} \cos\left[\frac{2\pi z}{P}(lN_0-m)+m\phi\right] \cos\left[\frac{2\pi}{P}(lN_0-m)\delta\right] \right.$$
$$\left. - \sum_{m=1,\text{odd}}^{lN_0-1} \sin\left[\frac{2\pi z}{P}(lN_0-m)+m\phi\right] \sin\left[\frac{2\pi}{P}(lN_0-m)\delta\right] \right\}$$
$$\times \frac{1}{lN_0-m} \mathcal{H}_{m,(2\pi/P)(lN_0-m)} K_m\left[\frac{2\pi}{P}(lN_0-m)\rho\right]$$
$$+ \frac{4qN_0}{b\pi} \sum_{l=-\infty}^{\infty} \left\{ \sum_{m=\max[2,2-lN_0],\text{even}}^{\infty} \cos\left[\frac{2\pi z}{P}(lN_0+m)-m\phi\right] \cos\left[\frac{2\pi}{P}(lN_0+m)\delta\right] \right.$$
$$\left. - \sum_{m=\max[1,1-lN_0],\text{odd}}^{\infty} \sin\left[\frac{2\pi z}{P}(lN_0+m)-m\phi\right] \sin\left[\frac{2\pi}{P}(lN_0+m)\delta\right] \right\}$$
$$\times \frac{1}{lN_0+m} \mathcal{H}_{m,(2\pi/P)(lN_0+m)} K_m\left[\frac{2\pi}{P}(lN_0+m)\rho\right]. \tag{A33}$$

APPENDIX B: POTENTIAL OF A POINT CHARGE IN A CYLINDRICALLY SYMMETRIC DIELECTRIC MEDIUM

Here we obtain the electrostatic potential due to a single point charge q embedded in a medium consisting of three cylindrically concentric dielectric layers, as depicted in Fig. (1b). The charge is located on the inner boundary separating the first and second layers and corresponds to a single phosphate group in this application. We are to solve the Maxwell equations in cylindrical coordinates, $x=(\rho,\phi,z)$:

$$\nabla\cdot\mathbf{D}=0, \quad \text{and} \quad \nabla\times\mathbf{E}=\mathbf{0}, \tag{B1}$$

inside each layer, where $\mathbf{D}=\epsilon(\rho)\mathbf{E}$, subject to the boundary conditions ($\hat{\rho}$ is the outward unit radial vector)

$$(\mathbf{D}_2-\mathbf{D}_1)\cdot\hat{\boldsymbol{\rho}}=4\pi\sigma(\phi,z)\ ,$$
$$(\mathbf{E}_2-\mathbf{E}_1)\times\hat{\boldsymbol{\rho}}=0\ , \tag{B2}$$

at $\rho=b$, and

$$(\mathbf{D}_3-\mathbf{D}_2)\cdot\hat{\boldsymbol{\rho}}=0\ ,$$
$$(\mathbf{E}_3-\mathbf{E}_2)\times\hat{\boldsymbol{\rho}}=0\ , \tag{B3}$$

at $\rho=d$, where

$$\epsilon(\rho)=\begin{cases}\epsilon_1\ , & 0\le\rho<b\\ \epsilon_2\ , & b\le\rho<d\\ \epsilon_3, & d\le\rho<\infty\end{cases} \tag{B4}$$

is a piecewise constant dielectric "constant." The surface charge distribution (located at $\rho=b$) is denoted by σ. Since $\nabla\times\mathbf{E}=\mathbf{0}$ everywhere (i.e., for $0\le\rho<\infty$), we can derive the field from a potential $\mathbf{E}=-\nabla\Phi$, and thus reduce the problem to one of solving Laplace's equation $\nabla^2\Phi=0$ inside each layer subject to the above boundary conditions (B2) and (B3).

As discussed in Sec. II, of the number of techniques which are used for solving electrostatic boundary-value problems, only the Green-function method is suited for solving the field from a helical charge distribution. This requires knowledge of the single-charge potential to which we now turn. We can immediately write down the most general Ansätze which solve Laplace's equation (in cylindrical coordinates) in each of the three regions by generalizing the representation of the Green function in cylindrical coordinates [16]:

$$\Phi_1=\sum_{m=0}^{\infty'}\int_0^\infty dk\ I_m(k\rho)\mathcal{F}_{1(m,k)}(\phi,z) \tag{B5}$$

for $0\le\rho<b$,

$$\Phi_2=\sum_{m=0}^{\infty'}\int_0^\infty dk[r_{(m,k)}I_m(k\rho)+K_m(k\rho)]\mathcal{F}_{2(m,k)}(\phi,z) \tag{B6}$$

for $b<\rho<d$, and

$$\Phi_3=\sum_{m=0}^{\infty'}\int_0^\infty dk\ K_m(k\rho)\mathcal{F}_{3(m,k)}(\phi,z) \tag{B7}$$

for $d<\rho<\infty$, where I_m and K_m are the two linearly independent modified Bessel functions of order m and

$$\begin{aligned}\mathcal{F}_{i(m,k)}(\phi,z)=&A_i(m,k)\cos(m\phi)\sin(kz)\\ &+B_i(m,k)\cos(m\phi)\cos(kz)\\ &+C_i(m,k)\sin(m\phi)\sin(kz)\\ &+D_i(m,k)\sin(m\phi)\cos(kz)\end{aligned} \tag{B8}$$

uses a complete set of basis functions for expanding any function on a cylinder. The prime on the sums indicates division of the $m=0$ modes by a factor of $\frac{1}{2}$. The higher-mode terms are doubled in number due to the fact that the cosine is an even function. Instead of writing the zero mode as a separate term, we choose to include it in the expansions and in order to do so, we must remember to divide it by 2, relative to the higher modes. Periodicity in the angle ϕ implies a discrete Fourier expansion in that variable, while the z dependence is handled with a continuous Fourier series. The form in (B8) results from taking the product of the separate basis functions for each independent variable (ϕ and z) on the cylinder. Note that the regularity of the potential Φ_1 at the origin, $\rho=0$, and the finiteness of Φ_3 at infinity have already been incorporated in the above expansions.

It is straightforward to work out the relations among the various expansion coefficients (B8) which follow from the boundary conditions. From (B2) we have

$$\left[-\frac{\partial\Phi_2}{\partial z}+\frac{\partial\Phi_1}{\partial z}\right]_{\rho=b}=\frac{1}{\rho}\left[-\frac{\partial\Phi_2}{\partial\phi}+\frac{\partial\Phi_1}{\partial\phi}\right]_{\rho=b}=0$$

and

$$\left[-\epsilon_2\frac{\partial\Phi_2}{\partial\rho}+\epsilon_1\frac{\partial\Phi_1}{\partial\rho}\right]_{\rho=b}=4\pi\sigma\ ,$$

which imply

$$I_m(kb)\begin{bmatrix}A_1\\B_1\\C_1\\D_1\end{bmatrix}=[r_{(m,k)}I_m(kb)+K_m(kb)]\begin{bmatrix}A_2\\B_2\\C_2\\D_2\end{bmatrix} \tag{B9}$$

and

$$\begin{aligned}\epsilon_1 I'_m(kb)\begin{bmatrix}A_1\\B_1\\C_1\\D_1\end{bmatrix}-\epsilon_2[r_{(m,k)}I'_m(kb)+K'_m(kb)]\begin{bmatrix}A_2\\B_2\\C_2\\D_2\end{bmatrix}\\ =\frac{4\pi}{k}\begin{bmatrix}\sigma_{CS}\\\sigma_{CC}\\\sigma_{SS}\\\sigma_{SC}\end{bmatrix}\ ,\end{aligned} \tag{B10}$$

where the prime indicates differentiation with respect to the arguments and we have expanded the surface charge distribution in terms of the same complete set as used for the $\mathcal{F}_i$, that is,

$$\begin{aligned}\sigma(\phi,z)=\sum_{m=0}^{\infty'}\int_0^\infty dk\ &\sigma_{CS}(m,k)\cos(m\phi)\sin(kz)\\ &+\sigma_{CC}(m,k)\cos(m\phi)\cos(kz)\\ &+\sigma_{SS}(m,k)\sin(m\phi)\sin(kz)\\ &+\sigma_{SC}(m,k)\sin(m\phi)\cos(kz)\ .\end{aligned} \tag{B11}$$

Similarly, from (B3) we have

$$\left[-\frac{\partial\Phi_3}{\partial z}+\frac{\partial\Phi_2}{\partial z}\right]_{\rho=d}=\frac{1}{\rho}\left[-\frac{\partial\Phi_3}{\partial\phi}+\frac{\partial\Phi_2}{\partial\phi}\right]_{\rho=d}=0$$

and

$$\left[-\epsilon_3\frac{\partial\Phi_3}{\partial\rho}+\epsilon_2\frac{\partial\Phi_2}{\partial\rho}\right]_{\rho=d}=0\ ,$$

so that

$$K_m(kd)\begin{bmatrix}A_3\\B_3\\C_3\\D_3\end{bmatrix}=[r_{(m,k)}I_m(kd)+K_m(kd)]\begin{bmatrix}A_2\\B_2\\C_2\\D_2\end{bmatrix} \tag{B12}$$

and

$$\epsilon_3K'_m(kd)\begin{bmatrix}A_3\\B_3\\C_3\\D_3\end{bmatrix}=\epsilon_2[r_{(m,k)}I'_m(kd)+K'_m(kd)]\begin{bmatrix}A_2\\B_2\\C_2\\D_2\end{bmatrix}\ . \tag{B13}$$

The solution of the boundary conditions is easily obtained. We find that

$$r_{(m,k)}=\frac{(\epsilon_2-\epsilon_3)K'_m(kd)K_m(kd)}{\epsilon_3I_m(kd)K'_m(kd)-\epsilon_2I'_m(kd)K_m(kd)}\ , \tag{B14}$$

while

$$\begin{bmatrix}A_1\\B_1\\C_1\\D_1\end{bmatrix}=\frac{\frac{4\pi}{k}[r_{(m,k)}I_m(kb)+K_m(kb)]}{(\epsilon_1-\epsilon_2)r_{(m,k)}I'_m(kb)I_m(kb)+[\epsilon_1I'_m(kb)K_m(kb)-\epsilon_2K'_m(kb)I_m(kb)]}\begin{bmatrix}\sigma_{CS}\\\sigma_{CC}\\\sigma_{SS}\\\sigma_{SC}\end{bmatrix}\ , \tag{B15}$$

$$\begin{bmatrix}A_2\\B_2\\C_2\\D_2\end{bmatrix}=\frac{\frac{4\pi}{k}I_m(kb)}{(\epsilon_1-\epsilon_2)r_{(m,k)}I'_m(kb)I_m(kb)+[\epsilon_1I'_m(kb)K_m(kb)-\epsilon_2K'_m(kb)I_m(kb)]}\begin{bmatrix}\sigma_{CS}\\\sigma_{CC}\\\sigma_{SS}\\\sigma_{SC}\end{bmatrix}\ , \tag{B16}$$

and

$$\frac{A_3}{A_2}=\frac{B_3}{B_2}=\frac{C_3}{C_2}=\frac{D_3}{D_2}=\left[1+r_{(m,k)}\frac{I_m(kd)}{K_m(kd)}\right]\ . \tag{B17}$$

The expansion coefficients are now completely specified in terms of the given surface charge density σ. If we specialize to a point charge q located on the boundary point (b,ϕ',z') separating the first and second dielectric layers, then

$$\sigma(\phi,z)=\frac{q}{b}\delta(\phi-\phi')\delta(z-z')\ . \tag{B18}$$

The moments [taken with respect to the expansion (B8)] of the point charge are calculated from (inverse) Fourier-sine and Fourier-cosine transforms:

$$\begin{bmatrix}\sigma_{CC}(m,k)\\\sigma_{CS}(m,k)\\\sigma_{SC}(m,k)\\\sigma_{SS}(m,k)\end{bmatrix}=\frac{1}{\pi^2}\frac{q}{b}\begin{bmatrix}\cos(m\phi')\cos(kz')\\\cos(m\phi')\sin(kz')\\\sin(m\phi')\cos(kz')\\\sin(m\phi')\sin(kz')\end{bmatrix}\ . \tag{B19}$$

Defining

$$\mathcal{I}_{m,k}=\frac{r_{(m,k)}I_m(kb)+K_m(kb)}{(\epsilon_1-\epsilon_2)r_{(m,k)}I'_m(kb)I_m(kb)+[\epsilon_1I'_m(kb)K_m(kb)-\epsilon_2K'_m(kb)I_m(kb)]}\ , \tag{B20}$$

$$\mathcal{B}_{m,k}=\frac{I_m(kb)}{(\epsilon_1-\epsilon_2)r_{(m,k)}I'_m(kb)I_m(kb)+[\epsilon_1I'_m(kb)K_m(kb)-\epsilon_2K'_m(kb)I_m(kb)]}\ , \tag{B21}$$

$$\mathcal{K}_{m,k}=\mathcal{B}_{m,k}\left[1+r_{(m,k)}\frac{I_m(kd)}{K_m(kd)}\right]\ , \tag{B22}$$

in terms of which the potential in each dielectric layer is given by

$$\Phi_1(\rho,\phi,z)=\frac{4q}{b}\frac{1}{\pi}\sum_{m=0}^{\infty'}\int_0^\infty\frac{dk}{k}\mathcal{I}_{m,k}I_m(k\rho)\cos(k[z-z'])\cos(m[\phi-\phi']) \tag{B23}$$

for $0 \leq \rho < b$, while

$$\Phi_2(\rho,\phi,z) = \frac{4q}{b}\frac{1}{\pi}\sum_{m=0}^{\infty'}\int_0^\infty \frac{dk}{k}\mathcal{B}_{m,k}(r_{(m,k)}I_m(k\rho)+K_m(kp))\cos(k[z-z'])\cos(m[\phi-\phi']) \tag{B24}$$

for $b \leq \rho < d$, and

$$\Phi_3(\rho,\phi,z) = \frac{4q}{b}\frac{1}{\pi}\sum_{m=0}^{\infty'}\int_0^\infty \frac{dk}{k}\mathcal{K}_{m,k}K_m(k\rho)\cos(k[z-z'])\cos(m[\phi-\phi']) \tag{B25}$$

for $d \leq \rho < \infty$.

As a check on our calculations, we note that for equal-ϵ limit, $\epsilon_1=\epsilon_2=\epsilon_3\equiv\epsilon$, $r_{(m,k)}\to 0$, and we recognize the Wronskian factor $\mathcal{W}[I_m(w),K_m(w)]=-1/w$ appearing in the coefficient functions (B20)–(B22). In this limit, this is equivalent to pushing the ϵ_1-ϵ_2 boundary layer into the origin and the ϵ_2-ϵ_3 boundary out to infinity. So Φ_3 vanishes while Φ_1 and Φ_2 can be combined into a single manifestly symmetric expression $\Phi(\mathbf{x},\mathbf{y})=\Phi(\mathbf{y},\mathbf{x})$ with range $0\leq\rho<\infty$:

$$\Phi(\mathbf{x},\mathbf{y}) = \frac{4q}{\epsilon}\frac{1}{\pi}\sum_{m=0}^{\infty'}\int_0^\infty dk I_m(k\rho_<)K_m(k\rho_>)\cos(k[z-z'])\cos(m[\phi-\phi']) , \tag{B26}$$

where $\rho_<$ ($\rho_>$) is the smaller (larger) of the magnitudes $|\mathbf{x}|$ and $|\mathbf{y}|$, and Φ is the (unique) solution (i.e., Green function) of Poisson's equation,

$$\nabla_x^2\Phi(\mathbf{x},\mathbf{y}) = -\frac{4\pi q/\epsilon}{\rho}\delta(\rho-b)\delta(\phi-\phi')\delta(z-z') . \tag{B27}$$

[1] T. L. Hill, Arch. Biochem. Biophys. **57**, 229 (1955).

[2] B. Pullman and A. Pullman, Prog. Nucl. Acids Res. **9**, 327 (1969); A. Pullman and B. Pullman, Q. Rev. Biophys. **14**, 289 (1981).

[3] A. Katchalsky, Pure Appl. Chem. **26**, 327 (1971).

[4] J. Schellman, Biopolymers **16**, 1415 (1977).

[5] G. S. Manning, Q. Rev. Biophys. **11**, 179 (1978); Acc. Chem. Res. **12**, 443 (1979).

[6] M. Fixman, J. Chem. Phys. **70**, 4995 (1979).

[7] D. W. R. Gruen, S. Marcelja, and B. A. Pailthrope, Chem. Phys. Lett. **82**, 315 (1981).

[8] E. Clementi and G. Corongiu, Biopolymers **21**, 763 (1982).

[9] M. LeBret and B. Zimm, Biopolymers **23**, 287 (1984).

[10] D. C. Rau, B. Lee, and V. A. Parsegian, Proc. Natl. Acad. Sci. **81**, 2621 (1984); S. Leiken, D. Leiken, D. C. Rau, and V. A. Parsegian, Phys. Rev. A **44**, 5272 (1991).

[11] Y. Tominaga *et al.*, J. Chem. Phys. **83**, 5972 (1986).

[12] N. J. Tao, S. M. Lindsay, and A. Rupprecht, Biopolymers **26**, 171 (1987); **27**, 1655 (1988); **28**, 1019 (1989).

[13] G. Edwards, G. Ying, and J. Tribble, Phys. Rev. A **45**, R8344 (1992).

[14] W. Saenger, *Principles of Nucleic Acid Structure* (Springer Verlag, Berlin, 1984).

[15] See, e.g., G. Binning, Bull. Am. Phys. Soc. **31**, 217 (1986); T. P. Beebe, Jr. *et al.*, Science **243**, 370 (1989); S. M. Lindsay *et al.*, *ibid.* **244**, 1063 (1989); J. Biomol. Struct. Dyn. **7**, 279 (1989).

[16] J. D. Jackson, *Classical Electrodynamics,* 2nd ed. (Wiley, New York, 1975).

[17] J. M. Eyster and E. W. Prohofsky, Phys. Rev. Lett. **38**, 371 (1977).

[18] V. K. Saxena and L. L. Van Zandt, Phys. Rev. A **45**, 7610 (1992).

[19] *Handbook of Mathematical Functions,* edited by M. Abramowitz and I. A. Stegun (Dover, New York, 1970).

[20] V. Renugopalakrishnan, A. V. Lakshminarayanan, and V. Sasisekharan, Biopolymers **10**, 1159 (1971).

[21] M. J. Lighthill, *Fourier Analysis and Generalised Functions* (Cambridge University Press, Cambridge, England, 1970).

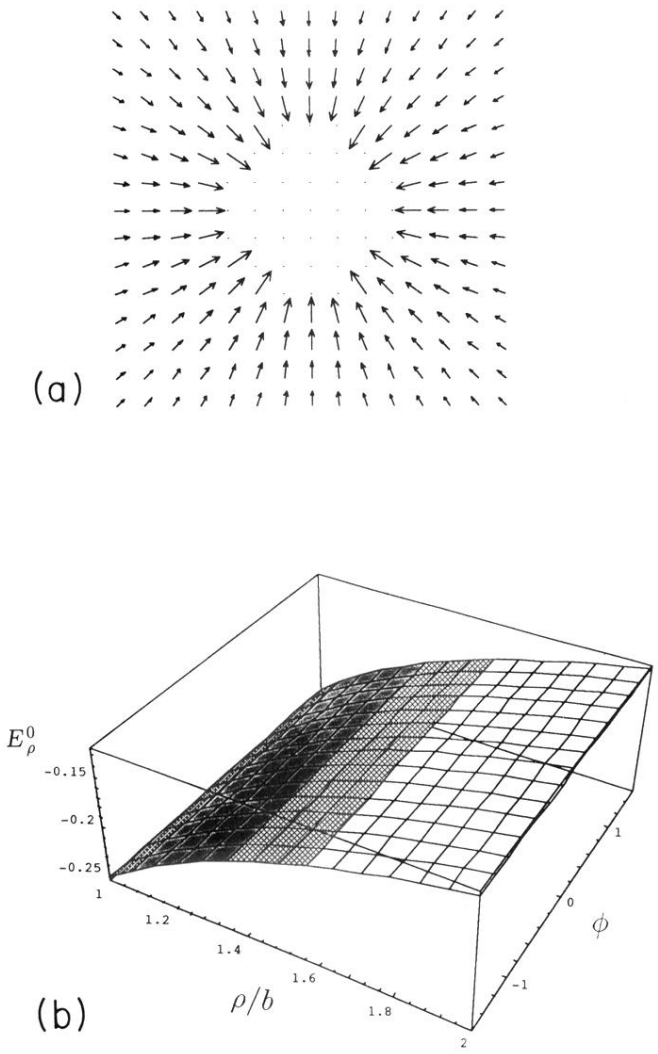

FIG. 2. Plot of the electric field of the leading term in $\mathbf{E}_\rho, \mathbf{E}^0_\rho$: (a) is a vector plot and (b) is a surface plot of the $z=0$ plane. Note that in (b) the ρ axis is normalized by b.

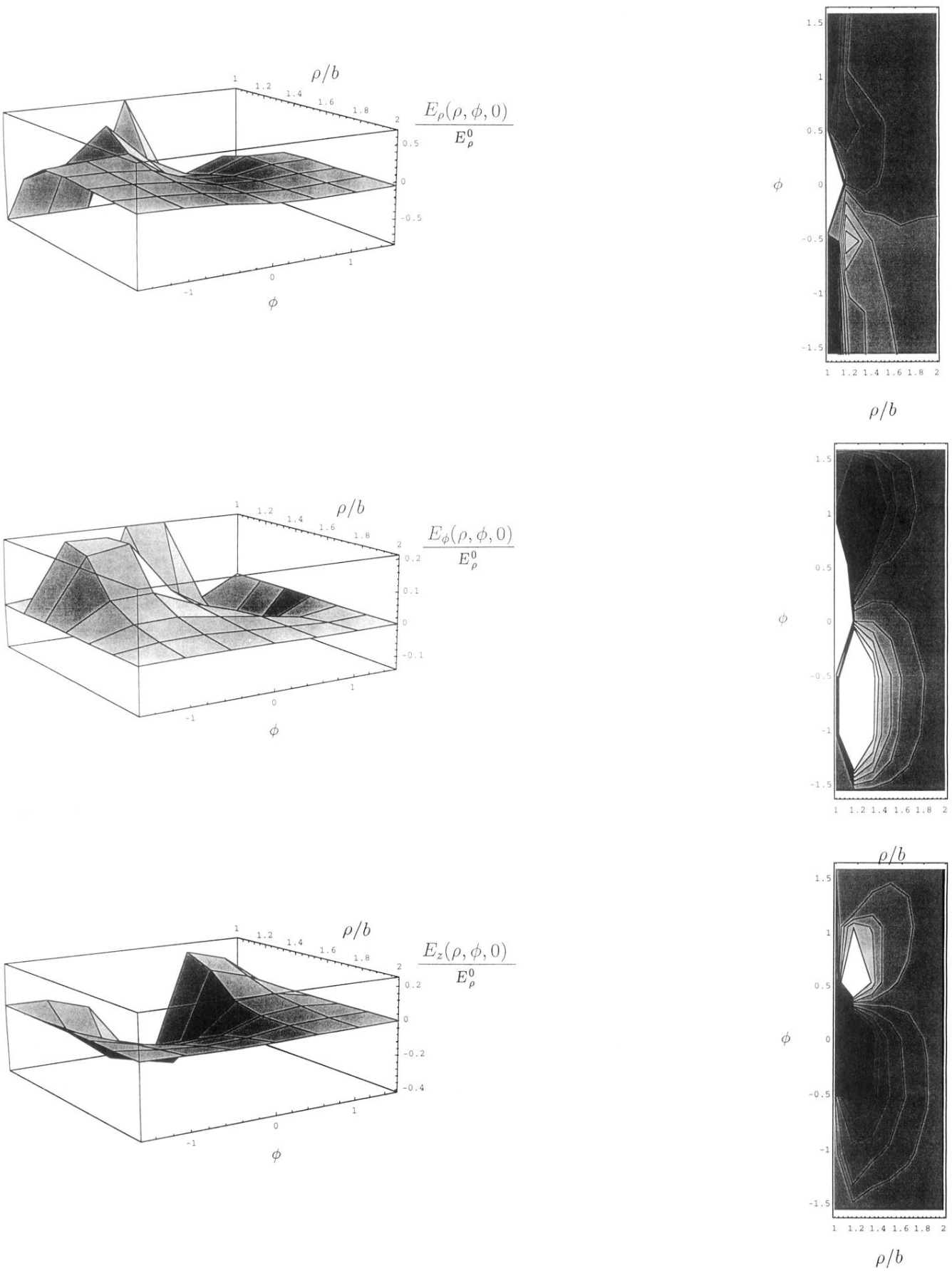

FIG. 3. Surface and contour plots of the components of the correction terms of the electric field in the $z=0$ plane. Note that the intensities of the components are relative to the intensity of the line-charge or zero-mode term E_ρ^0 as shown in Fig. 2.

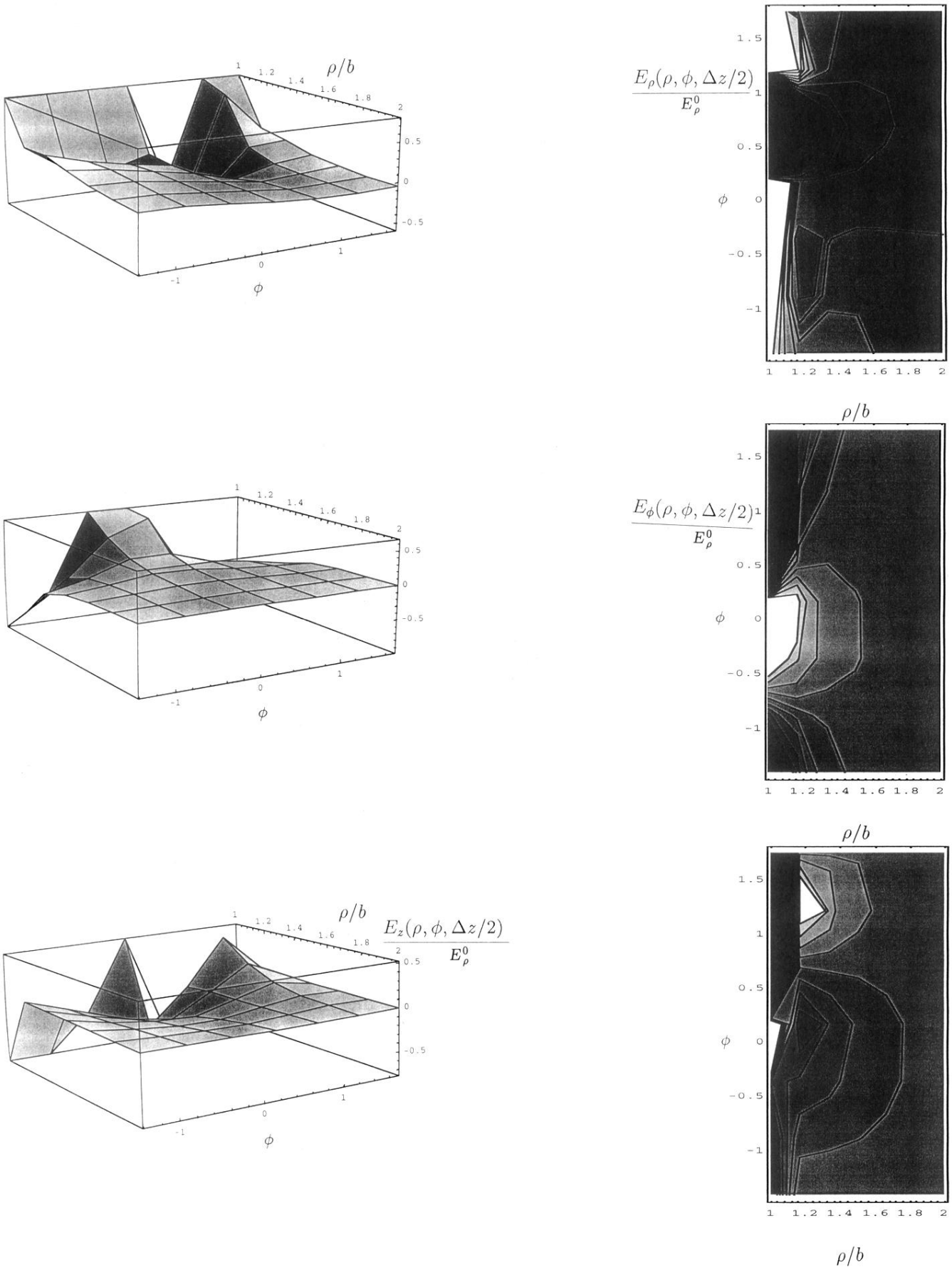

FIG. 4. Surface and contour plots of the components of the correction terms of the electric field in the $z = \Delta z/2$ plane.